Journal of the European Ceramic Society 15 (1995) 787 794

0955-2219(95)00042-9
0955-2219/95/$9.50

Preparation of Dispersed Zirconia Barium Aluminosilicate Composites

A. Nordmann, Y.-B. Cheng* & B. C. Muddle

Department of Materials Engineering, Monash University, Clayton, Victoria, 3168, Australia

(Received 18 May 1994; revised version received 7 February 1995; accepted 14 February 1995)

Abstract

The potential for preparing a ZrO_2-containing ceramic composite based on barium feldspar ($BaAl_2Si_2O_8$) using the reaction sintering of zircon has been investigated. It is demonstrated that, through the reaction of $ZrSiO_4$, Al_2O_3 and $BaCO_3$ above 1400°C, a distribution of ZrO_2 particles in a $BaO{\cdot}Al_2O_3{\cdot}2SiO_2$ matrix can be achieved. A glassy phase rich in Si and Ba surrounds the zirconia particles and infiltrates the grain boundaries of the polycrystalline feldspar matrix. The tendency of the ZrO_2 particles to agglomerate within the matrix can be reduced by incorporating additional silica into the reaction, while limited stabilisation of tetragonal ZrO_2 can be achieved by additions of Y_2O_3 which partition between the ZrO_2 and the glassy boundary phase.

Introduction

Zircon ($ZrSiO_4$) is a natural mineral resource known to react with certain oxides to produce a dispersion of zirconia particles within ceramic or glass–ceramic matrices. The reaction of zircon with alumina results, for example, in a ZrO_2–mullite composite material, while the reaction of zircon with alumina and magnesia or alumina and calcia produces ZrO_2-containing cordierite and anorthite, respectively.[2–5] These composite materials, obtained by the reaction sintering method in which consolidation of individual particles is accompanied by a chemical reaction, have often been shown to possess high thermal stability and improved fracture toughness, the latter being a direct consequence of the transformation toughening effect associated with the included ZrO_2 particles.[7]

Barium aluminosilicates, particularly the celsian polymorphs of $BaO{\cdot}Al_2O_3{\cdot}2SiO_2$, display oxidation resistance and refractory characteristics commensurate with the properties required of high temperature materials.[8–10] The orthorhombic (α) and hexagonal (β) phases of hexacelsian ($BaAl_2Si_2O_8$) possess thermal expansion coefficients of $7{\cdot}1 \times 10^{-6}$/°C and $8{\cdot}0 \times 10^{-6}$/°C, respectively,[11] while the monoclinic phase, simply termed celsian, has a melting point of 1760°C and a thermal expansion coefficient as low as $2{\cdot}29 \times 10^{-6}$/°C.[11] Zirconia has a thermal expansion coefficient of $6–10 \times 10^{-6}$/°C[12] which is comparable to that of the hexacelsian polymorphs and is therefore expected to minimise the thermal expansion mismatch within a composite material comprised of hexacelsian and zirconia. Such thermal properties, coupled with the high melting point of ZrO_2 (2680°C) suggest that barium aluminosilicates and zirconia are an ideal combination from which to fabricate high temperature materials. A recent study has indicated that a barium aluminosilicate containing up to 40 mol% ZrO_2 can be prepared via a sol–gel process.[13] However, the desire to utilise a natural resource in the form of zircon in the present work has led to the choice of reaction sintering as an alternative processing route. Reaction sintering is becoming increasingly attractive as a ceramic processing technique because of its simplicity and cost efficiency, and reaction sintering of zircon is a particularly effective means of dispersing zirconia grains into ceramic matrices. The current work was undertaken to investigate the possibility of forming a zirconia-containing barium feldspar composite material using the reaction sintering of zircon and assuming the following stoichiometric reaction:

$$2ZrSiO_4 + BaCO_3 + Al_2O_3 \rightarrow 2ZrO_2 + BaO{\cdot}Al_2O_3{\cdot}2SiO_2 + CO_2 \uparrow \quad (1)$$

Experimental Procedures

The starting powders used were $ZrSiO_4$ (Cerac 99% pure, average particle size approximately 3·5 μm), $BaCO_3$ (AJAX Chemicals, 99% pure), SiO_2

* To whom correspondence should be addressed.

(AJAX Chemicals, precipitated) and Al_2O_3 (AJAX Chemicals). Stabilisation of ZrO_2 was achieved through the addition of Y_2O_3 (Cerac 99·9% pure). The powders were hand-mixed for 20 min in an alumina mortar and pestle with a small amount of isopropanol added for lubrication. Batches of about 2·5 g were compressed uniaxially in a compaction die to produce pellets approximately 14 mm in diameter. The pellets were placed in a high purity alumina crucible and fired in a rapid heating furnace in which temperatures of up to 1600°C could be achieved in 80 min, and a cooling rate of 20°C/min was employed. The mercury displacement method was used to determine the bulk density of sintered samples.

Phase identification for the sintered samples was carried out using X-ray diffraction (XRD) on a Rigaku Geigerflex diffractometer with Cu K_α radiation and a Ni filter. Samples for scanning electron microscopy (SEM) were mounted, ground on SiC paper and polished prior to being carbon coated and examined in a JEOL JSM840A scanning electron microscope operating at 20 kV. Samples for transmission electron microscopy (TEM) were cut, polished, ion-beam milled to perforation, carbon coated and then examined in a Philips EM420 TEM operating at 120 kV and equipped with an EDAX PV9900 energy dispersive X-ray spectrometer.

Results and Discussion

Sample preparation

Initial nominal compositions of the samples prepared are shown in Table 1. The progress of reaction sintering, the densification behaviour of the samples and the microstructures produced were studied in detail using a variety of techniques.

Crystalline phases

The reaction sequence of the system was studied by obtaining XRD spectra from samples sintered for 2 h at temperatures of 1000–1600°C at 100°C intervals. The positions of characteristic peaks at each of the given temperatures allowed for the identification of phases as the reaction progressed. With changes in the sintering temperature the starting powders reacted to form intermediate phases as well as the final products. By comparing the intensities of peaks corresponding to the reactants it was possible to obtain an indication of when these phases disappeared. Similarly, the emergence of new phases could also be monitored as the reaction progressed, and the relative intensities of corresponding characteristic peaks were used to define approximately the proportions of the phases as a function of sintering temperature. Representative XRD spectra of samples sintered for 2 h at 1300 and 1600°C are shown in Fig. 1(a) and (b), respectively, while the results in Fig. 2 illustrate the relative proportions of phases detected at different sintering temperatures.

The onset of zircon dissociation is evident at approximately 1100°C. This compares favourably

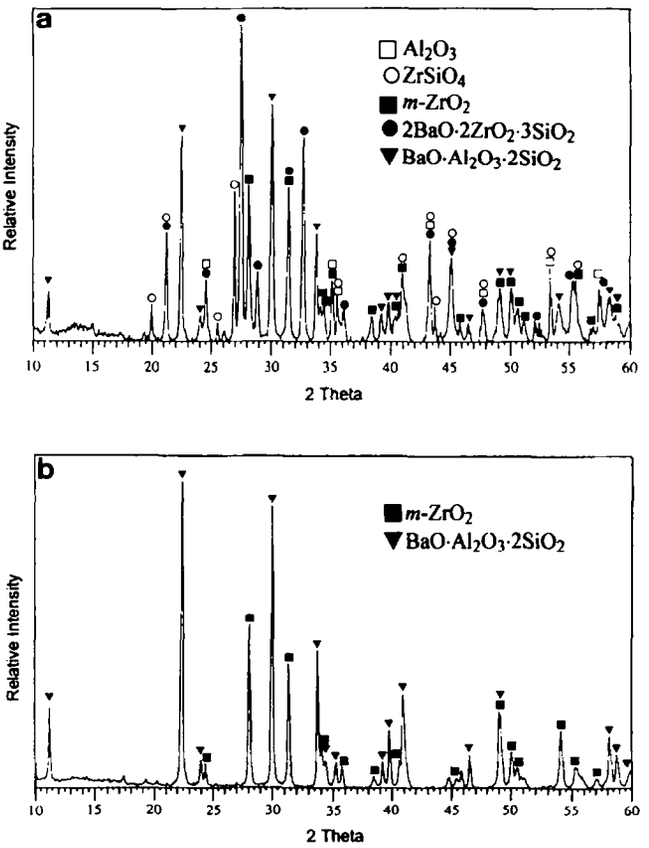

Fig. 1. XRD traces of samples sintered for 2 h at (a) 1300°C and (b) 1600°C.

Table 1. Nominal compositions of samples prepared (wt%)

Sample	*$ZrSiO_4$*	*Al_2O_3*	*$BaCO_3$*	*SiO_2*	*Y_2O_3*
1—Reaction 1	55·1	15·3	29·6	—	—
2—Reaction 2	33·8	18·9	36·4	11·1	—
3—Yttria stabilised (4%)	54·2	15·0	29·2	—	1·5
4—Yttria stabilised (8%)	53·3	14·8	28·7	—	3·1
5—Yttria stabilised (12%)	52·4	14·6	28·2	—	4·8

Reaction (1) is defined by the stoichiometric equation while reaction (2) incorporates additional silica into the reaction. Compositions 1 and 2 correspond to reactions (1) and (2), respectively, while compositions 3, 4 and 5 are free of additional silica and lead to sintered products in which the Y_2O_3 concentration corresponds to 4, 8 and 12 wt% of the anticipated ZrO_2 content.

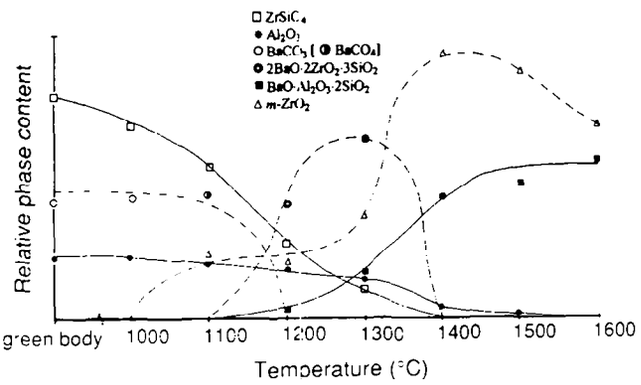

Fig. 2. Reaction sequence showing approximately the relative proportion of major phases present as a function of sintering temperature.

with the dissociation temperature of pure zircon of 1670°C, indicating that the presence of the other components significantly lowers the temperature at which the constituents, ZrO_2 and SiO_2, are obtained. The dissociation of zircon at 1100°C is accompanied by the appearance of monoclinic zirconia, m-ZrO_2. The SiO_2 obtained from the dissociation is not detected as a crystalline phase and is thus assumed to exist in an amorphous state. At this temperature, barium carbonate has undergone a structural change from $BaCO_3$ to a phase identified as $BaCO_4$,[14] but no evidence of decomposition of this phase was observed.

At 1200°C, the zircon content has further diminished and the barium carbonate has completely decomposed. The ZrO_2 and BaO thereby attained manifest themselves in the formation of an intermediate phase, $2BaO{\cdot}2ZrO_2{\cdot}3SiO_2$,[15] which also utilises the SiO_2 formed at lower temperatures. Furthermore, a slight reduction in Al_2O_3 is observed at this temperature, a barium aluminosilicate phase (hexacelsian) starts to emerge and a barium silicate phase, $2BaO{\cdot}3SiO_2$,[16] is also detected. However, since the latter phase was only observed at 1200°C it is not represented by a separate curve in Fig. 2.

At 1300°C, the Al_2O_3 and $ZrSiO_4$ contents continue to decrease, the transitory barium silicate phase has disappeared and the proportions of m-ZrO_2, hexacelsian and $2BaO{\cdot}2ZrO_2{\cdot}3SiO_2$ have increased. On heating to 1400°C, the decomposition of $ZrSiO_4$ is essentially complete and the Al_2O_3 content shows a marked reduction. This coincides with a maximum in the ZrO_2 content and increasing formation of hexacelsian. These observations may be explained by the complete dissociation of the barium zirconium silicate ($2BaO{\cdot}2ZrO_2{\cdot}3SiO_2$), which reacts with Al_2O_3 and thereby allows for the formation of hexacelsian.

At 1500°C only a trace of Al_2O_3 is detected, with the dominant phases being the reaction products, hexacelsian and ZrO_2. Zirconia is present only as the monoclinic phase since no stabilising oxide has been added at this stage to allow for the stabilisation of tetragonal zirconia. It is noted that a reduction in the ZrO_2 content occurs and this may be explained by the dissolution of ZrO_2 in the residual liquid. The solubility of ZrO_2 increases with increasing temperature and hence a further reduction in ZrO_2 is observed at 1600°C. By 1600°C, the initial powders have completely reacted to form hexacelsian and m-ZrO_2.

The detection of hexacelsian in these samples is interesting and perhaps raises questions concerning the existing understanding of this material. It is commonly reported that the barium aluminosilicate of composition $BaAl_2Si_2O_8$ may exist as one of three crystallographic phases: α-hexacelsian (orthorhombic), β-hexacelsian (hexagonal) and celsian (monoclinic).[8–11] Monoclinic celsian is stable thermodynamically below 1590°C, whereas β-hexacelsian is stable above 1590°C. However, the transformation between β-hexacelsian and celsian occurs sluggishly, so that β-hexacelsian may persist as a metastable phase below 1590°C.[8] Furthermore, it has been reported that at approximately 300°C, β-hexacelsian undergoes a rapid, reversible displacive transformation to metastable orthorhombic α-hexacelsian and that this transformation is accompanied by a 3–4% volume expansion, which is large enough to potentially cause deterioration of the material during cooling.[17] The α and β forms of hexacelsian are based on similar lattices and, given the similarity in interplanar spacings for the two phases, it proved impossible to distinguish between them in the current samples using X-ray diffraction.[18] However, there was little metallographic evidence of significant cracking in the matrix of the sintered samples suggesting that the β-hexacelsian may have been retained as a metastable phase, and that the transformation to orthorhombic α-hexacelsian may have been suppressed on cooling to room temperature.

The preferential formation of metastable hexacelsian rather than monoclinic celsian has previously been ascribed to structural differences.[8] The high symmetry hexagonal and orthorhombic forms may be described in terms of infinite two-dimensional hexagonal sheets consisting of two layers of $(Si,Al)O_4$ tetrahedra, whereas the low symmetry celsian consists of a three-dimensional structure in which the four vertices of the tetrahedra are shared. In both structures, some substitution of Al for Si occurs in the tetrahedra and charge compensation by Ba is provided through its location either between the sheets, in the case of hexacelsian, or in the larger interstices of the celsian structure. The

two-dimensional high symmetry forms therefore have lower kinetic barriers for nucleation and are consequently formed first. Nevertheless, with a suitable additive it may be possible to stabilise monoclinic celsian in these materials.[19]

Densification

The sintering behaviour was further monitored by measuring the density of the sintered samples as a function of temperature and the results are presented in Fig. 3. The initial reduction in the density up to 1200°C may be the result of the decomposition of $BaCO_3$. The CO_2 gas evolved during this decomposition will, if trapped in the sample, expand with further heating, and thereby cause an expansion of the specimen. With continued heating, chemical reaction begins accompanied by particle coalescence and sample shrinkage occurs. A significant increase in the rate of densification is observed above 1300°C and a maximum density of 3·52 g/cm^3 is obtained at 1500°C. It is thought that the melting of the intermediate phase ($2BaO{\cdot}2ZrO_2{\cdot}3SiO_2$) above 1300°C provides a low temperature eutectic liquid which facilitates the rapid densification. The relatively lower density measured at 1600°C is attributed to the bloating effect prevalent in these samples, a phenomenon which may be a result of the instability of the low temperature eutectic liquid phase. In addition, the transformation of zirconia from tetragonal to monoclinic symmetry on cooling produced cracks in samples sintered above 1200°C and this may also have contributed to a reduction in the measured density. The trends observed in the densification process were substantiated by dilatometry measurements, although the results obtained are not presented here.

Scanning electron micrographs were obtained at various stages of the reaction sequence to illustrate particle arrangement and distributions at each temperature. Since little microstructural change occurred on sintering below 1300°C, only those samples prepared at the higher sintering temperatures ($T \geq 1300$°C) where the most significant changes occurred, are represented in Fig. 4.

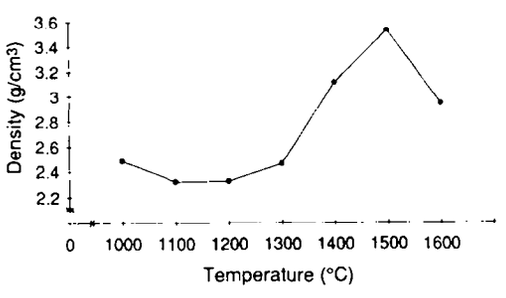

Fig. 3. Density as a function of temperature for samples prepared according to reaction 1. Rapid densification is seen to take place at temperatures immediately above 1300°C.

The emergence of a liquid phase occurs at 1300°C (arrowed, Fig. 4(a)); however, since only a small amount of this phase is formed, no significant densification is achieved at this temperature. At 1400°C, Fig. 4(b), there are significant pores present but individual grains of starting powder are no longer distinguished. The lighter contrast regions in Fig. 4(b) are ZrO_2-rich and comprise clusters of small spheroidal grains with a morphology typical of a product forming in the presence of a liquid phase. The microstructural observations are consistent with both density and X-ray results which suggest that chemical reaction and densification are significantly accelerated between 1300 and 1400°C. At 1500°C, Fig. 4(c), the dispersion of ZrO_2 particles is clearly evident, although the tendency to form agglomerates is common. At 1600°C, Fig. 4(d), the reaction is essentially complete and spherical ZrO_2 particles, between 1 and 3 μm in diameter, remain as agglomerates within the feldspar matrix.

The results to this stage support the feasibility of using a reaction sintering approach to fabricate a ZrO_2/hexacelsian composite material. A significant porosity is observed in all samples and the ZrO_2 particles remain in localised clusters, often in association with pores. In addition, as a result of the tetragonal (*t*) to monoclinic (*m*) transformation within the ZrO_2 grains on cooling, these particles are of monoclinic symmetry with the ensuing cracks in the samples being a direct consequence of the volume expansion associated with this transformation.

Stabilisation of ZrO_2

In order to prevent cracking of the samples, it was necessary to suppress the spontaneous *t* to *m* transformation in the ZrO_2 particles on cooling through the addition of a suitable stabilising oxide. As shown in Table 1, the compositions were adjusted to incorporate additions of Y_2O_3 corresponding to 4, 8 and 12 wt% of the expected ZrO_2 content, and subsequent sintering was performed at 1500°C for 2 h. According to the ZrO_2–Y_2O_3 phase diagram,[20] at 1500°C the 4 wt% composition is located in the tetragonal phase field; the 8 and 12 wt% compositions lie in the tetragonal/cubic phase field. Provided that the Y_2O_3 partitions to the ZrO_2 during reaction sintering, the precipitation of transformable metastable *t*-ZrO_2 might therefore be expected on cooling and hence phase transformation toughening may become possible at room temperature.

In contrast to the yttria-free samples, all the samples with additional yttria displayed negligible cracking after sintering. As shown in Table 2, X-ray diffraction suggested that increasing fractions

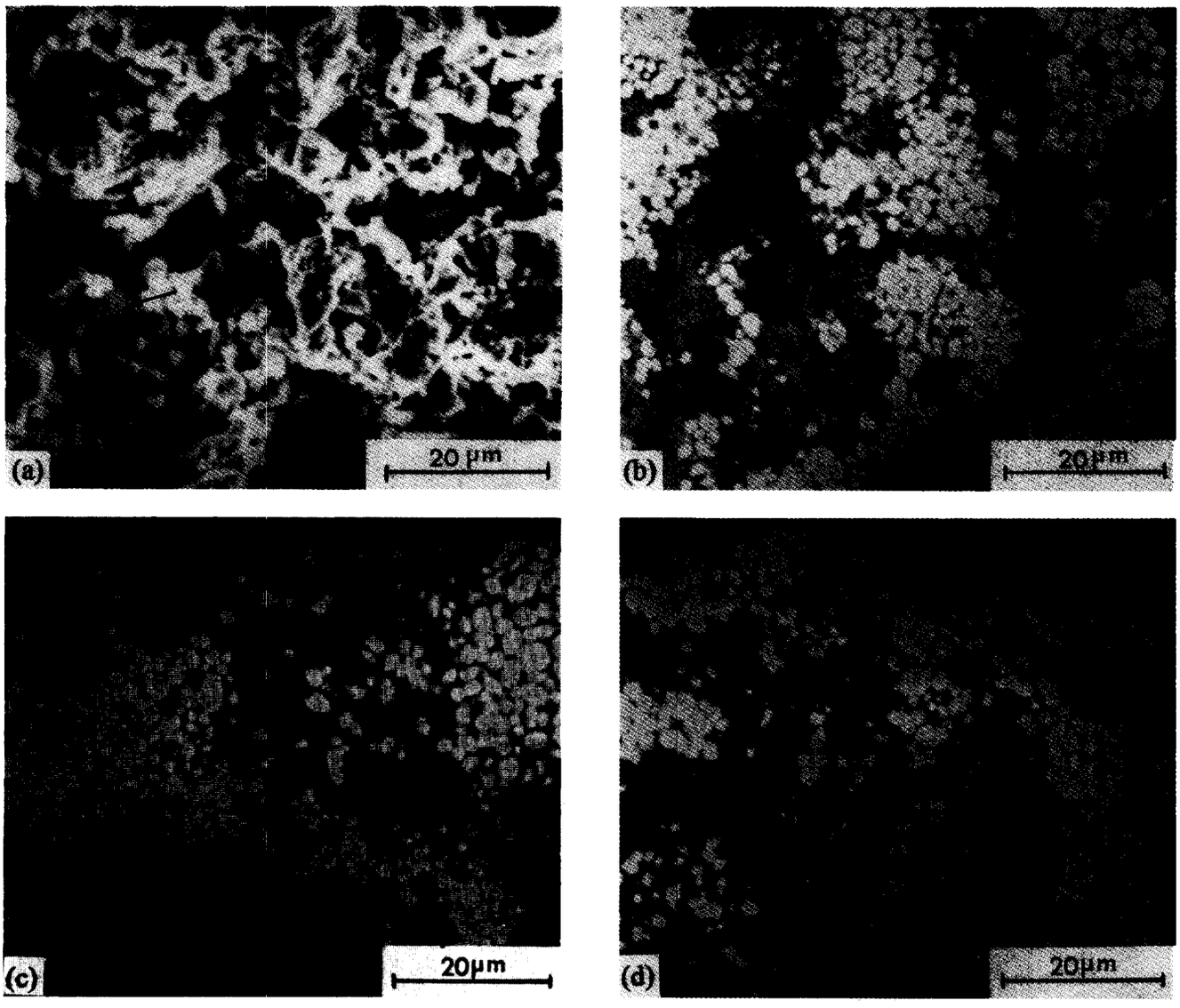

Fig. 4. SEM images depicting the microstructures obtained when sintering for 2 h at (a) 1300°C (b) 1400°C (c) 1500°C and (d) 1600°C.

of zirconia were stabilised as tetragonal phase with increasing yttria content. Moreover, in samples containing 4 and 8 wt% Y_2O_3, the ratio of monoclinic to tetragonal zirconia was found to be increased after grinding the samples to a fine powder using a mortar and pestle, see Table 2. Since the mechanical stresses associated with this grinding are comparable to the stresses located around a crack tip, these results are indicative of the potential for a toughening increment to be achieved through the stress-induced transformation of zirconia dispersed within the composite. It is noted that analysis of the XRD data was complicated by overlap between the (111) t-ZrO_2 peak and what is either the (112) peak of α-hexacelsian or the (102) peak of β-hexacelsian. However, a comparison of peak intensities corresponding to m- and t-ZrO_2 is still useful, since the intensity of the feldspar peaks should be unaffected by grinding and any changes in the peak intensity at this location can be attributed entirely to changes in the fraction of t-ZrO_2.

Table 2. Ratio of monoclinic to tetragonal zirconia in the yttria-modified samples before and after grinding. Samples were sintered for 2 h at 1500°C

Y_2O_3 content	$I_m(11\bar{1})/I_t(111)$ before grinding	$I_m(11\bar{1})/I_t(111)$ after grinding
4%	29/100	41/100
8%	0/100	9/100
12%	0/100	0/100

Microstructural observation

A sample containing 4 wt% Y_2O_3 and sintered at 1500°C for 2 h was further characterised using transmission electron microscopy and energy dispersive X-ray spectroscopy (EDXS). As shown in Fig. 5(a), the microstructure contained local clusters of spheroidal ZrO_2 particles dispersed in an amorphous matrix. The domain substructure of the particles and the corresponding selected area diffraction pattern, Fig. 5(b), confirm that they are m-ZrO_2. The substructure of approximately twin-related domains arises during the displacive t to m transformation, in order to accommodate the shear

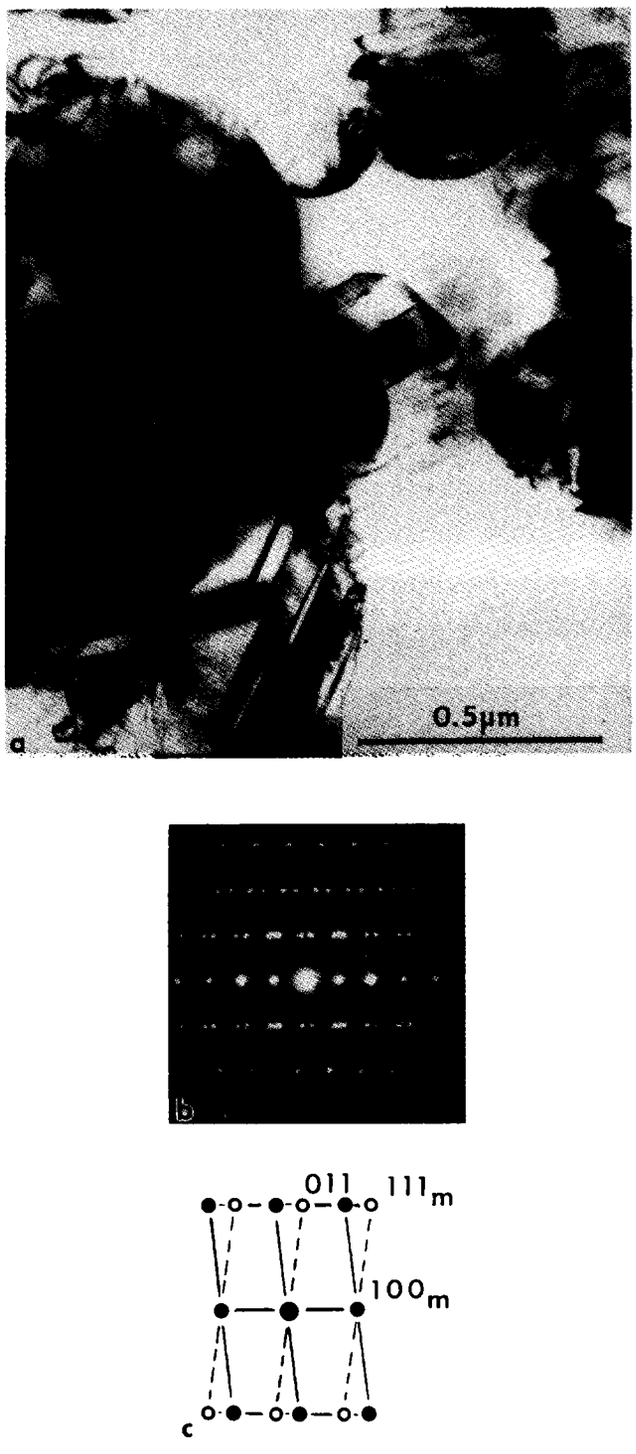

Fig. 5. (a) Bright field TEM micrograph of a sample containing 4 wt% Y_2O_3 and sintered for 2 h at 1500°C; (b) corresponding SAED pattern from single ZrO_2 particle, and (c) schematic solution to pattern containing two variants of the monoclinic phase twin-related about $(100)_m$. The zone axis is $[0\bar{1}1]_m$.

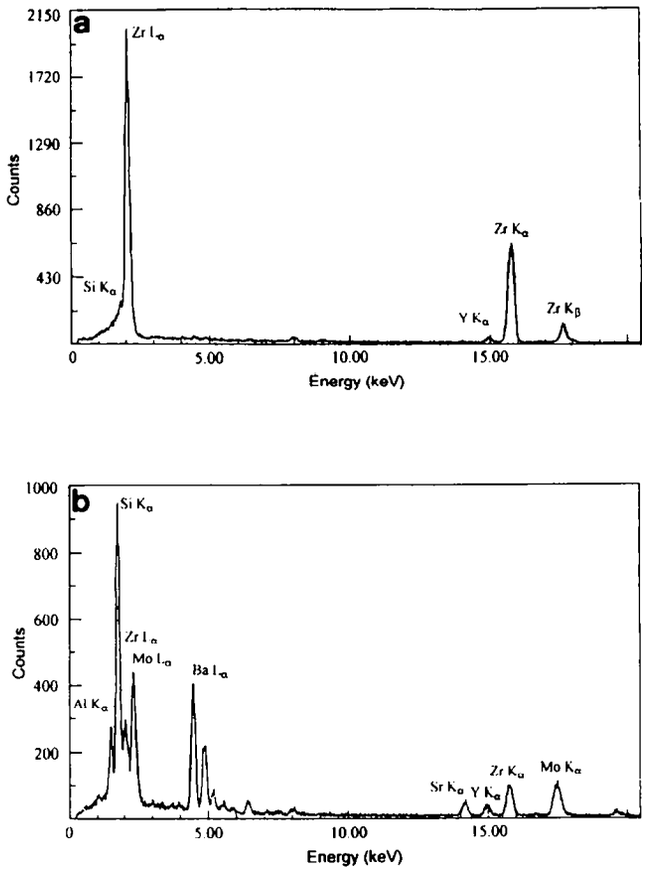

Fig. 6. EDX spectra from a sample containing 4 wt% Y_2O_3, sintered for 2 h at 1500°C. Spectra were recorded from (a) a zirconia grain shown in Fig. 5(a) and; (b) the glassy region seen in Fig. 5(a). The molybdenum recorded in Figure 5(b) is a contaminant resulting from ion-beam milling.

component of transformation. The absence of extensive microcracking around the particles indicates that the residual misfit strains around the particles may be accommodated by the glassy matrix.

X-ray microanalysis, Fig. 6(a), indicated that detectable concentrations of Y_2O_3 were present within the ZrO_2 grains. However, there was also a significant concentration of Y_2O_3 in the surrounding amorphous phase, indicating that an excess of Y_2O_3 may be necessary to stabilise the ZrO_2 as tetragonal phase. The detection of a significant fraction of tetragonal phase in X-ray diffraction patterns from this sample, and the failure to observe tetragonal phase in thin foil specimens, can probably be attributed to the tetragonal to monoclinic transformation occurring during preparation of the thin foil specimens upon relaxation of matrix constraint.

Figure 7 includes bright field images recorded from matrix regions of the same sample. In this case the structure is polycrystalline and the mixture of elongated and equiaxed grains were identified as metastable hexacelsian using electron microdiffraction. However, the diffraction patterns recorded from such grains, Fig. 8, could commonly be interpreted as being from either the high temperature hexagonal β form or the low temperature orthorhombic α phase. The pattern in Fig. 8(a) may, for example, be indexed as representing either a hexagonal $[2\bar{1}\bar{1}0]$ zone axis pattern or a [100] orthorhombic zone, while that in Fig. 8(b) is either a $[\bar{2}4\bar{2}3]$ zone axis pattern from the hexagonal phase or a $[\bar{2}01]$ pattern from the orthorhombic α. In the absence of detailed information on the crystal structures for the two phases it proved

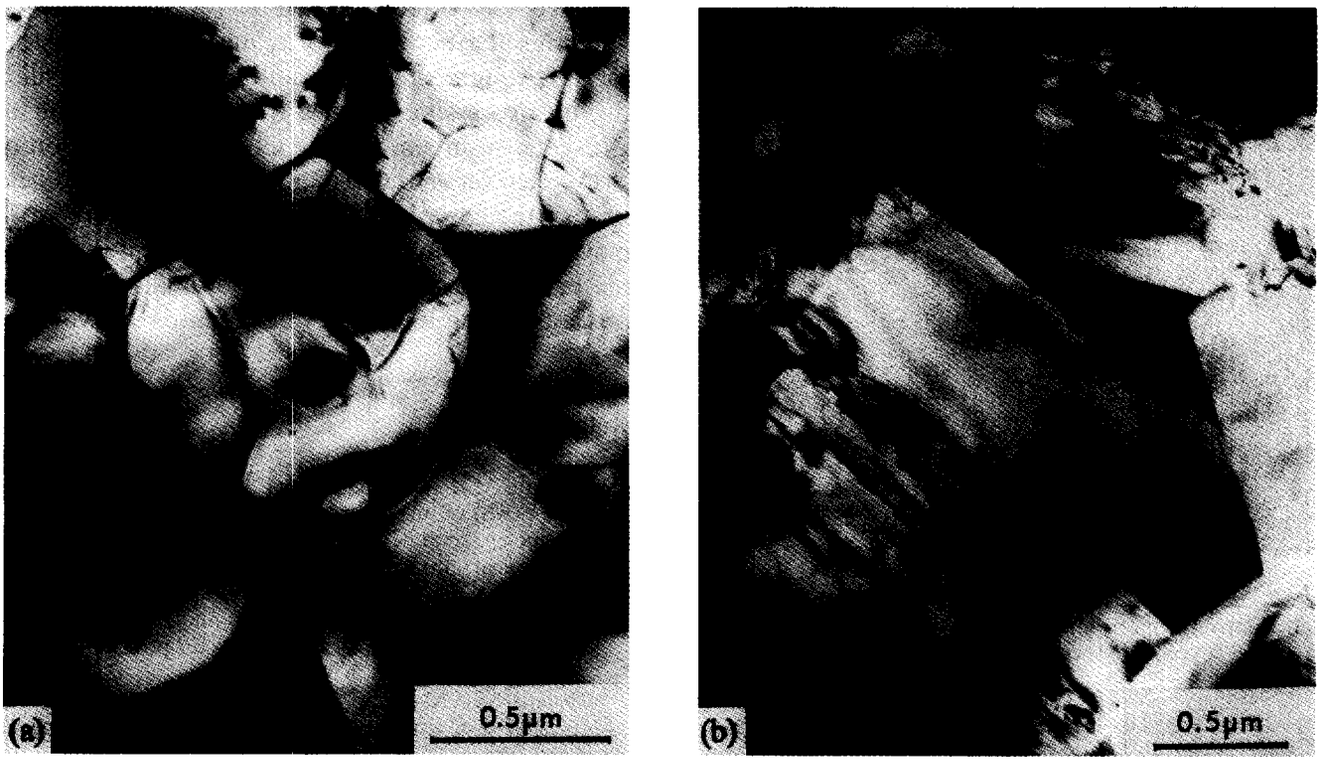

Fig. 7. Bright field TEM images showing (a) equiaxed and (b) elongated grains of hexacelsian.

impossible to identify zone axes for which patterns might be distinguishable for the two structures and thus impossible, in this preliminary study, to distinguish between the phases using electron diffraction. However, there was little or no evidence in the microstructure of the matrix of a solid state displacive transformation to the orthorhombic α-hexacelsian, or of the cracking or microcracking that might be expected to accompany such a transformation involving a 3–4% volume change. It is thus suggested that the hexagonal β-hexacelsian may have been retained as the dominant metastable phase at ambient temperature.

The micrographs of Fig. 7 indicate that the grains of hexacelsian were separated by a thin film of the same glassy phase as that surrounding the zirconia particles, and that there were pockets of glassy phase at grain triple junctions. Diffraction patterns recorded from such triple junctions contained diffuse rings consistent with an amorphous structure, and EDX spectra from such pockets, Fig. 6(b), indicated that the phase was Si-rich, with a high content of Ba. The composition is consistent with a glassy phase that is liquid during sintering to facilitate consolidation and the spheroidal form of the ZrO_2 grains is characteristic of the morphology that would be expected to develop during liquid phase sintering.

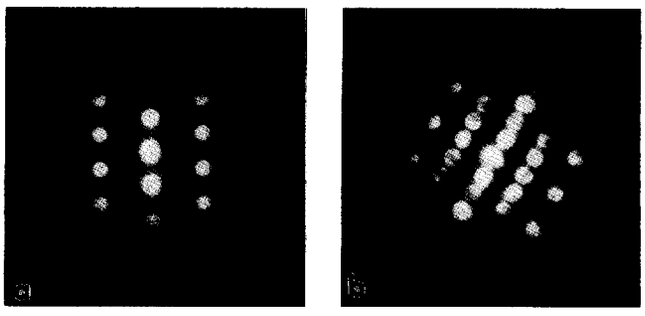

Fig. 8. Electron microdiffraction patterns recorded from hexacelsian grains which may be indexed as representing (a) a hexagonal $[2\bar{1}\bar{1}0]$ zone axis pattern or a [100] orthorhombic zone; and (b) a $[\bar{2}4\bar{2}3]$ zone axis pattern from the hexagonal β phase or a $[\bar{2}01]$ pattern from the orthorhombic α hexacelsian.

Effect of additional SiO_2

The stoichiometric reaction (1) yields a product with a molar ratio of zirconia to feldspar of 2:1. On the basis that the excess zirconia concentration may contribute to the inhomogeneous dispersion of zirconia agglomerates, additional SiO_2 was added in an attempt to improve the sinterability and homogeneity of the composites, assuming a reaction of the form:

$$ZrSiO_4 + BaCO_3 + Al_2O_3 + SiO_2 \rightarrow ZrO_2 + BaO{\cdot}Al_2O_3{\cdot}2SiO_2 + CO_2 \uparrow \quad (2)$$

It was anticipated that addition of SiO_2 would serve to form extra low temperature eutectic liquid phase and a comparatively lower zirconia concentration. A further series of samples was thus prepared under similar processing conditions, but with the composition of Sample 2 given in Table 1.

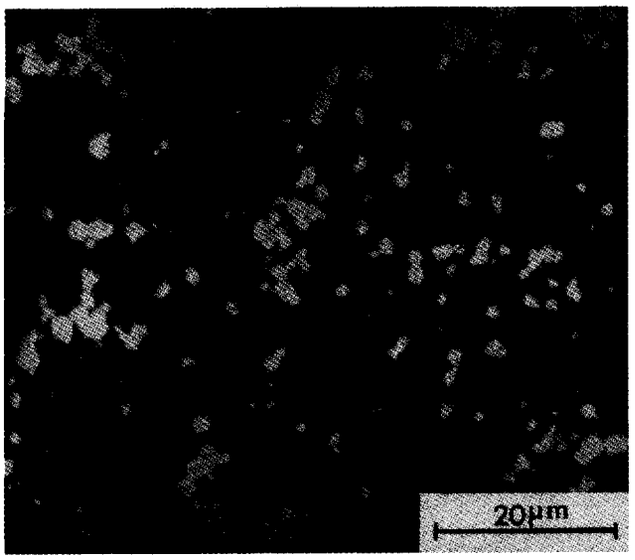

Fig. 9. SEM micrograph of Sample 2 sintered at 1500°C for 2 h, showing a more uniform distribution of ZrO_2 particles compared with that shown in Fig. 4.

The scanning electron micrograph recorded from the resulting sample is shown in Fig. 9 and indicates that the effective reduction in zircon content has resulted in a lower volume fraction and more uniform distribution of zirconia particles within the matrix. However, the improved distribution of the ZrO_2 particles seems to occur at the expense of the densification achieved. In fact, the highest density attained for the silica modified reaction was 2·87 g/cm^3 when sintering was carried out at 1500°C for 2 h. A possible explanation of this effect may lie in the origin of the silica. A finer, more uniform dispersion of amorphous SiO_2 produced from the dissociation of zircon may permit a more uniform formation of liquid phase that in turn facilitates densification more readily.

Conclusions

Reaction sintering of zircon with alumina and barium carbonate produces a composite material comprising distributed ZrO_2 in a continuous barium feldspar matrix. The spheroidal particles of ZrO_2 are in clusters surrounded by an amorphous phase rich in Si and Ba, and there is evidence that this glassy phase also infiltrates the grain boundaries of the polycrystalline feldspar matrix. Electron and X-ray diffraction results suggest that the matrix consists of either hexagonal (β) or orthorhombic (α) forms of hexacelsian ($BaO{\cdot}Al_2O_3{\cdot}2SiO_2$), or a combination of these two phases. Yttria added during processing partitions in part to the ZrO_2 allowing a significant fraction of the ZrO_2 to be retained as tetragonal phase at room temperature and thus the potential for a measure of transformation toughening. The addition of extra silica during processing reduces the volume fraction of ZrO_2 and results in a more uniform distribution of ZrO_2 particles. However, in this case the densification of the composite is less effective. Future work may focus on improving the dispersion of the zirconia particles by the use of attrition milling or other mixing–milling techniques of the initial powders.

References

1. Anseau, M. R., Leblud, C. & Cambier, F., Reaction sintering (RS) of mixed zircon-based powders as a route for producing ceramics containing zirconia with enhanced mechanical properties. *J. Mater. Sci. Lett.*, **2** (1983) 366–70.
2. Pilate, P. & Cambier, F., Synthesis and reaction sintering with alumina of plasma sprayed zircon powder. *Silicates Industriels*, **7–8** (1986) 95–8.
3. Holmström, M., Chartier, T. & Boch, P., Reaction-sintered ZrO_2-mullite composites. *Mater. Sci. Engng.*, **A109** (1989) 105–9.
4. Boch, P. & Giry, J. P., Preparation of zirconia-mullite ceramics by reaction sintering. *Science of Sintering*, **20**(2/3) (1988) 141–8.
5. Descamps, P., Sakaguchi, S., Poorteman, M. & Cambier, F., High-temperature characterisation of reaction-sintered mullite-zirconia composites. *J. Am. Ceram. Soc.*, **74**(10) (1991) 2476–81.
6. Cheng, Y. -B. & Thompson, D. P., Zirconia toughening of cordierite and anorthite glass ceramics. *British Ceramic Proceedings — Complex Microstructures*, ed. R. Stevens & D. Taylor, **42** (1989) 149–58.
7. Garvie, R. C., Hannink, R. H. J. & Pascoe, R. T., Ceramic steel? *Nature*, **258** (1975) 703–4.
8. Drummond, C. H., Lee, W. E., Bansal, N. P. & Hyatt, M. J., Crystallization of a barium aluminosilicate glass. *Ceram. Engng. Sci. Proc.*, **10**(9–10) (1989) 1485–502.
9. Drummond, C. H., Crystallization behaviour and properties of $BaO{\cdot}Al_2O_3{\cdot}2SiO_2$ glass matrices. *Ceram. Engng. Sci. Proc.*, **11**(7–8) (1990) 1072–86.
10. Bansal, N. P. & Hyatt, M. J., Crystallization kinetics of $BaO{\cdot}Al_2O_3{\cdot}SiO_2$ glasses. *J. Mater. Res.*, **4**(5) (1989) 1257–65.
11. Moya Corral, J. S. & Garcia Verduch, A., The solid solution of silica in celsian. *Trans. J. Br. Ceram. Soc.*, **77** (1978) 40–4.
12. Green, D. J., Hannink, R. H. J. & Swain, M. V., *Transformation Toughening of Ceramics*. CRC Press Inc., Boca Raton, Florida, 1989, pp. 222–3.
13. Debsikdar, J. C., Effect of zirconia addition on crystallinity, hardness and microstructure of gel-derived barium aluminosilicate, $BaAl_2Si_2O_8$. *J. Mater. Sci.*, **27** (1992) 5320–4.
14. JCPDF card no. 3–659.
15. JCPDF card no. 25–1466.
16. JCPDF card no. 27–1035.
17. Yoshiki, B. & Matsumoto, K., High-temperature modification of barium feldspar. *J. Am. Cer. Soc.*, **34**(9) (1951) 283–6.
18. JCPDF card nos. 12–725, 12–726.
19. Chen, M., Lee, W. E. & James, P. F., Synthesis of monoclinic celsian glass-ceramics from alkoxides. *J. Non-Cryst. Solids.*, 147–148 (1992) 532–6.
20. Scott, H. G., Phase relationships in the zirconia-yttria system. *J. Mater. Sci.*, **10** (1975) 1527.